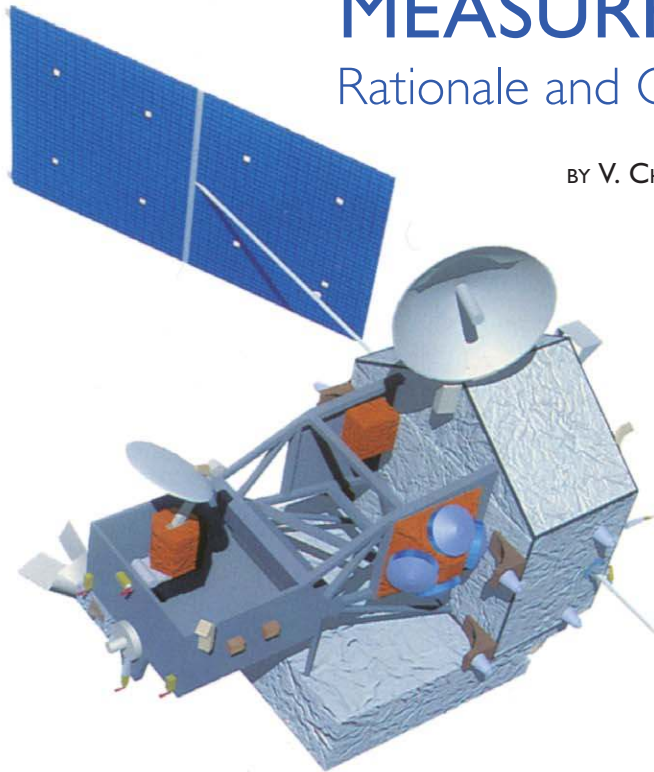# POTENTIAL ROLE OF DUAL-POLARIZATION RADAR IN THE VALIDATION OF SATELLITE PRECIPITATION MEASUREMENTS
Rationale and Opportunities

BY V. CHANDRASEKAR, ARTHUR HOU, ERIC SMITH, V. N. BRINGI, S. A. RUTLEDGE, E. GORGUCCI, W. A. PETERSEN, AND GAIL SKOFRONICK JACKSON

Ground based dual-polarization radars provide physical insight into the development and interpretation of spaceborne precipitation measurements

TRMM satellite. Source: NASA/Goddard Space Flight Center
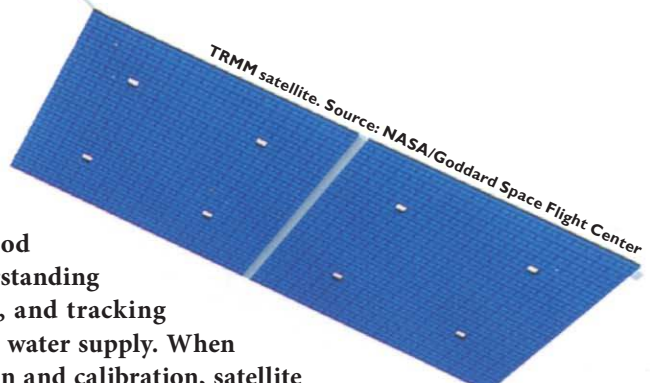
Reliable global quantitative precipitation measurement is critically important for a variety of applications, including flood forecasting, numerical weather prediction, understanding the evolution of hurricanes and severe storms, and tracking of long-term trends in global precipitation and water supply. When combined with comprehensive ground validation and calibration, satellite observations offer practical prospects for acquiring accurate and global datasets especially over oceans and remote regions. Since the advent of satellite sensing of clouds and precipitation there has been much progress in terms of instrumentation and algorithm development. The Tropical Rainfall Measuring Mission (TRMM), launched in 1997, represents an advanced active and passive remote sensing system to measure precipitation. Each precipitation satellite mission requires thorough ground validation to test instrument and algorithm performance. With the success of the TRMM and the plans for TRMM's successor mission, the Global Precipitation Measurement mission (GPM), the current era represents ▶

the "golden age" of microwave precipitation remote sensing (National Research Council 2006, 2007).

Yet, even with the success of TRMM, more complete coverage is needed, both spatially and temporally. TRMM only samples tropical precipitation (±35° latitude) and has an orbit period of about 92 min with an approximate repeat cycle of 40 days (Chang et al. 1999). Additional coverage is needed for short-term finescale applications such as hydrology, and for improving and validating GCM models. The Committee on Earth Observation Satellites (CEOS), the international coordinating body for earth observing satellite systems (available online at www.ceos.org), declared precipitation to be an important measurement and they identify GPM as a prototype of the Global Earth Observation System of Systems (GEOSS).

The GPM mission is an international satellite mission to provide accurate precipitation measurements around the globe every 2 to 4 h (available online at http://gpm.gsfc.nasa.gov). The GPM mission concept is centered on the deployment of a Core Observatory satellite with an active dual-frequency (Ka/Ku band) precipitation radar and a passive GPM Microwave Imager (GMI) with wideband (10–183 GHz) capabilities (Shimizu et al. 2006). The core satellite (±65° latitude) will serve as a precipitation physics observatory and will provide the calibration standard for a global constellation of dedicated and operational passive microwave sensors. The baseline GPM constellation is envisioned to comprise conically scanning radiometers such as GMI, *Global Change Observing Mission* (*GCOM*)-*W,* and Special Sensor Microwave Imager/Sounder (SSMIS), supplemented by cross-track sounders, such as Advanced Technology Microwave Sounder (ATMS) and Microwave Humidity Sensor (MHS) over land. GPM is currently a partnership between the National Aeronautics and Space Administration (NASA) and the Japan Aerospace Exploration Agency (JAXA), with opportunities for participation of additional partners via constellation satellites. The anticipated launch date of the GPM Core spacecraft is expected to occur in 2013.

GPM is a science mission with integrated applications goals for advancing the knowledge of the global water/energy cycle variability as well as improving weather, climate, and hydrological prediction capabilities through more accurate and frequent measurements of global precipitation. The dual-frequency precipitation radar (DPR) aboard the GPM core satellite is expected to improve our knowledge of precipitation processes relative to the single-frequency radar used in TRMM by providing greater dynamic range, more detailed information on microphysics, and better accuracies in rainfall and liquid water content retrievals. The DPR will be able to provide information on rain and snow distributions over a wide range of precipitation intensities (from ~0.2 to about 110 mm h^{-1}). This information will not only give us insight into microphysical processes but also provide bulk properties of the precipitation, such as water flux (rain rate) and water content. The dual-frequency returns will also allow us to distinguish regions of liquid, frozen, and mixed-phase precipitation. Overall, the combination of Ka and Ku bands should significantly improve the detection thresholds for light rain and snow relative to TRMM. The improved accuracy and more detailed microphysical information from the dual-wavelength radar can also be used to constrain the cloud model database to be used in simultaneous precipitation retrievals from the brightness temperature measurements by the multichannel radiometer on the GPM Core. These radiometric improvements should be transferable to the constellation radiometers where simultaneous radar data are not available.

Validation is an integral part of all satellite precipitation missions. The process of validation is a cross-cutting effort covering many areas all the way from sensor development to ending with the end users products. Ground validation helps to characterize errors, quantify measurement uncertainty, and, most importantly, provide insight into the physical and statistical basis of the retrieval algorithms. The GPM validation falls in the general class of validation and integration of information from a variety of spaceborne observing platforms with ground-based measurements and data assimilation efforts. For TRMM, the validation activity included elements

AFFILIATIONS: Chandrasekar, Bringi, and Rutledge—Colorado State University, Fort Collins, Colorado; Hou, Smith, and Skofronick Jackson—NASA Goddard Space Flight Center, Greenbelt, Maryland; Gorgucci—Istituto di Scienze dell' Atmosfera e del Clima (CNR), Rome, Italy; Petersen—NASA Marshall Space Flight Center, Huntsville, Alabama
CORRESPONDING AUTHOR: V. Chandrasekar, Colorado State University, 1373 Campus Delivery, Fort Collins, CO 80523-1373
E-mail: chandra@engr.colostate.edu

such as pointwise validation of spaceborne radar measurements, statistical validation of the precipitation products, and validation for understanding precipitation processes. For GPM, the traditional approaches are planned with the addition of validation sites designed specifically to 1) perform statistical validation of retrieved satellite surface precipitation products, 2) investigate precipitation processes, and 3) validate integrated hydrology applications.

Dual-polarization weather radar is a very powerful validation tool that can be used to address a number of important questions that arise in the validation process, especially those associated with precipitation microphysics and algorithm development. Beginning with the early introduction of circular polarization measurements by McCormick and Hendry (1975) and the subsequent advancement of linear polarization measurements by Seliga and Bringi (1976), polarization diversity radars have consistently advanced all three areas of interest for cross validation of spaceborne measurements, namely, the understanding of precipitation processes, calibration, and quantitative precipitation estimation (QPE). The introduction of differential phase measurements advanced the QPE applications (Seliga and Bringi 1978; Sachidananda and Zrnic 1987; Chandrasekar et al. 1990), whereas the microphysical characterization has advanced significantly to the level of producing hydrometeor classification products (Straka et al. 2000; Liu and Chandrasekar 1998, 2000; Vivekanandan et al. 1999). Dual-polarization radar measurements were also used to advance the radar calibration for quantitative applications, using the self-consistency principle of the polarization diversity measurements (Gorgucci et al. 1992; Scarchilli et al. 1996). Thus, the dual-polarization measurements have played a significant role in several areas of importance to cross validation of satellite observation of precipitation.

The following describes the various aspects of the dual-polarization weather radar specifically in the context of validating spaceborne precipitation estimates. This paper is organized as follows: the next section provides brief background on the dual-polarization weather radars, along with the discussion of various types of dual-polarization radar measurements. The different implementation of dual-polarization radars involves different technologies and they are also summarized. In the section "Application of dual-polarization radar to rainfall microphysical retrievals," the applications of dual-polarization radars for rainfall microphysical research is reviewed, especially in the context of spaceborne application. A brief background of

the TRMM program space-based measurement of precipitation is discussed in the section "Progress on validation of TRMM precipitation measurement with dual-polarization radars" along with the advancement made during the TRMM era in cross validation of satellite measurements. Potential applications of dual-polarimetric radar in the GPM era are summarized in section 5.

BACKGROUND. The fundamental science of polarimetric radar observations of precipitation can be described by the diagram in Fig. 1. The transmitted waveform propagates through precipitation media, is scattered back from the particles in the resolution volume, and after propagating back through precipitation media, is received by the radar. The propagation medium characteristics are described by the propagation matrix, whereas the backscatter properties are described by the scattering matrix of precipitation resolution volume. The early pioneering work at the National Research Council (NRC) in Ottawa by McCormick, Hendry, and colleagues focused on measuring the coherency matrix of precipitation at circular polarization (Bringi and Chandrasekar 2001). One of the major results that came out of the study was that they were not operating at the eigen-polarization states of the rain medium. The implication was that the polarization state keeps changing due to propagation through rain medium. This realization motivated the team led by Seliga and Bringi (1976) to operate at the eigen-polarization states of the rain medium, namely, the horizontal (H) and vertical (V) states. In addition, for simplicity and hardware considerations, Seliga and Bringi (1976) focused on an incomplete, but nevertheless microphysically relevant, set of measurements. They proposed two methods of obtaining polarization diversity measurements, namely, a) alternately switching the transmit polarization states between H and V polarization states, with copolar reception via a
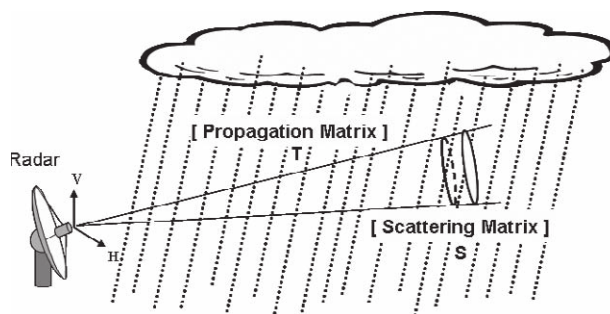

Fɪɢ. 1. Schematic of the propagation and backscatter in precipitation.

single receiver, and b) simultaneous transmission and reception (STAR) mode using dual-channel receivers. The late 1970s were prior to the digital revolution, and the alternate switching of polarization along with copolar signal reception with a single receiver was much cheaper to implement compared to the two-receiver mode of implementation. Subsequently, many research radar installations upgraded their radars to dual-polarization capability, including the University of Chicago–Illinois State Water Survey (CHILL) radar, National Center for Atmospheric Research (NCAR) CP-2, and the Chilbolton radar. Most of the activities in the United States were concentrated on making detailed copolar and cross-polar measurements and interpreting these data by developing simplified microphysical models.

In the meantime, in the late 1980s the research team at the German Aerospace Research Establishment (DLR) embarked on a fairly aggressive program to develop a polarization diversity radar to make measurements at arbitrary polarization states (Schroth et al. 1988). They also installed a unique polarization switch and polarizer such that the receive polarization states could be controlled independent of the transmit polarization states. By then several teams, including the DLR and Colorado State University–CHILL (CSU–CHILL), started pursuing the complete set of measurements from linear polarization states.

Though the initial Next Generation Weather Radars (NEXRAD) were not dual polarized, polarization research initiated at the National Severe Storms Laboratory (NSSL), along with the overwhelming results from other radar installations mentioned above, led to the deployment of a prototype dual-polarization radar for the U.S. National Weather Service (Doviak et al. 2000). Similarly, several European countries have initiated deployment of dual-polarization radars for operational applications, indicating the maturity of the science and applications (Parent et al. 2005). Commercial entities, including several stations in the broadcast meteorological sector, have also recognized the operational QPE benefits of dual-polarimetric radar and have begun upgrade to C-band dual-polarimetry [e.g., the joint University of Alabama at Huntsville (UAH)–WHNT-TV Advanced Radar for Meteorological and Operational Research (ARMOR) radar; Petersen et al. 2007]. Thus, dual-polarization radars have come a long way from early research to operational application. The Joint Polarization Experiment (JPOLE; Ryzhkov et al. 2005) evaluated the operational applications of dual-polarization radar from a weather service perspective and the potential demonstrated by the various observations of dual polarization since the early 1980s have resulted in a decision by the National Weather Service to upgrade the Weather Service radars [Weather Surveillance Radar-1988 Doppler (WSR-88D)] to dual polarization (available online at www.roc.noaa.gov).

In a conventional single-polarization radar the reflectivity factor is related to the backscatter cross section of the individual precipitation particles through the particle size distribution. The various parameters measured from the dual-polarization radars are essentially the various elements of the dual-polarization covariance matrix (DPCV) of precipitation (Bringi and Chandrasekar 2001). If a radar can measure all elements of the dual-polarization covariance matrix, then it is termed a fully polarimetric radar. Many dual-polarization radars measure only a subset of the elements of the dual-polarization covariance matrix. Most of the definitions of the various dual-polarization measurements are available in various research articles and textbooks (e.g., Bringi and Chandrasekar 2001). The equivalent radar reflectivity factor at each polarization is given by the diagonal elements of the covariance matrix, proportional to the volumetric radar cross section. An extension of this reflectivity measurement to dual polarization with the distinction of radar cross section of particles and reflectivities between horizontal and vertical polarization states results in the differential reflectivity (Z_{dr}). Here, Z_{dr} is defined as the ratio of reflectivities at horizontal and vertical polarization:

$$Z_{dr} = 10 \log_{10}\left(\frac{Z_h}{Z_v}\right), \qquad (1)$$

where Z_h, Z_v are the radar reflectivity factors measured at horizontal and vertical polarization. The copolar correlation coefficient is defined as the correlation between the radar-received signals at horizontal and vertical polarization; it is a complex number possessing a magnitude from zero to one and is denoted by the symbol ρ_{co} to indicate the copolar correlation coefficient.

In addition to measuring reflectivities at the same polarization state transmitted by the radar, the systems can be configured to measure the received power at the polarization state orthogonal to the transmitted polarization state. This was routinely accomplished in circular polarization operation (McCormick and Hendry 1975), but not common with linear polarization states. When the cross-polar power is measured

at the linear polarization state, then it is converted to an equivalent reflectivity factor and the ratio of copolar to crosspolar reflectivity is termed as linear depolarization ratio (LDR). Here, Z_h, Z_{dr}, and LDR are real (power) measurements, whereas ρ_{co} is complex, associated with a magnitude and a phase. As the electromagnetic wave from the radar propagates through precipitation, then the dual-polarization signals are modified due to propagation effects, such as differential attenuation and differential phase between the H and V polarization states. At radar frequencies where the attenuation is negligible such as S band, the main impact of propagation through precipitation is the differential phase. In the presence of propagation, the phase of ρ_{co} is modified as

$$\text{Arg}[\rho_{co}] = \phi_{dp} + \delta_{hv}, \qquad (2)$$

where φ_{dp} is the differential phase due to propagation, and δ_{hv} is the differential phase due to backscatter. The differential propagation phase is proportional to the water content along a rain path and is one of the important parameters measured by dual-polarization radar (Seliga and Bringi 1978; Jameson 1985).

The term dual-polarization radar does not uniquely refer to a specific radar configuration or a set of measurements. Several configurations of dual-polarization radars are available depending on the measurement goals and choice of polarization states. The covariance matrix forms a complete set of measurements and several research radars are configured for this measurement. In the early 1980s a number of single-polarized research radars were modified for limited dual-polarization measurements in the linear horizontal/vertical polarization states, for measuring differential reflectivity and later differential phase. These measurements involved only copolar signals, and the system requirements were not very stringent (Wang and Chandrasekar 2006) and significant practical results (such as rain-rate estimation and hail detection) were obtained fairly quickly.

The most general dual-polarization radar can be described as the system that has both polarization agility on transmit and polarization diversity on receive mode. Polarization agility refers to the ability to change the transmitted polarization state between any two orthogonal states on a pulse-to-pulse basis, whereas polarization diversity refers to the ability to simultaneously receive two orthogonal polarization states. Figure 2 shows the generalized block diagram of a two-transmitter/two-receiver system that supports both polarization diversity and agility, enabling fully polarimetric measurements. The CSU–CHILL
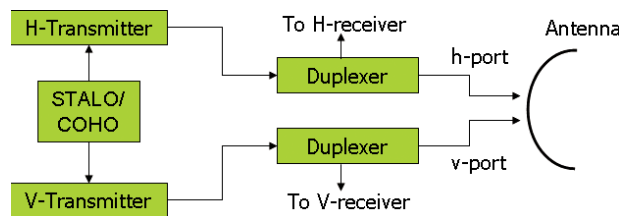

Fig. 2. Simple block diagram of the two-transmitter, two-receiver dual-polarized radar system.

radar has this configuration at 10-cm wavelength (S band) and more recently a similar configuration was implemented at the TRMM, ground validation facility at Okinawa [Communications Research Laboratory Okinawa Bistatic Polarimetric Radar (COBRA radar; Nakagawa et al. 2003)]. In addition, the various dual-polarization implementations at different installations can be broadly classified into three types, namely, 1) polarization agile/single-receiver systems, 2) polarization diversity systems, and 3) polarization agile dual-receiver systems. These types of systems have been described in detail in Bringi and Chandrasekar (2001).

APPLICATION OF DUAL-POLARIZATION RADAR TO RAINFALL MICROPHYSICAL RETRIEVALS. *Raindrop size distribution.* Dual-polarization radars have been used in retrieving droplet size distribution (DSD) parameters utilizing the relation between size and shape of raindrops. DSD is mainly used to describe the microphysical characteristics of the rain medium. The DSD also forms as the building block that is used to describe the remote sensing measurements of the rain medium. The most important polarization diversity radar measurements of the rain medium from radars at low-elevation angles are the differential reflectivity (Z_{dr}) and specific differential propagation phase (K_{dp}). These characteristic signatures are the consequence of a concentration of approximately oblate-shaped spheroidal raindrops coupled with a nearly vertical orientation of their symmetry axes forming an anisotropic propagation medium. The microphysical origin of these signatures is closely related to the raindrop size and shape distributions.

Raindrop shape. The equilibrium shape of a raindrop is determined by a balance of forces on the interface involving hydrostatic, surface tension and aerodynamic forces. Numerical model results of Beard and Chuang (1987) described the shape of raindrops as a function of size as shown in Fig. 3. Wind tunnel data of Pruppacher and Beard (1970) yielded a simple
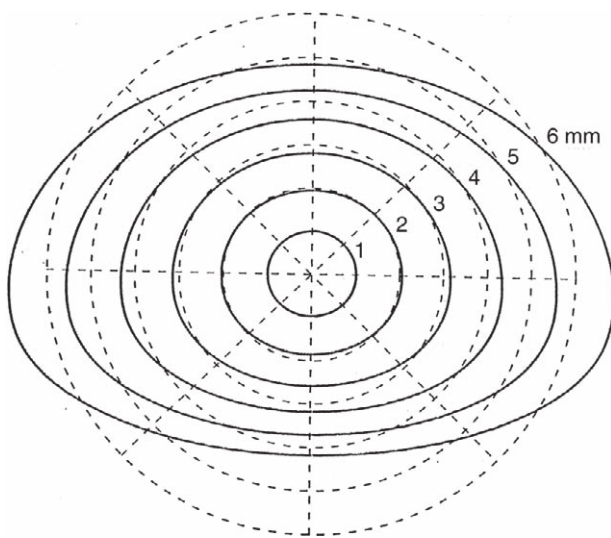
FIG. 3. Equilibrium drop shapes for drop diameters of 1–6 mm. From Beard and Chuang (1987).

Rotating linear polarization basis observations in rainfall showed that raindrops on the average fall with their symmetry axis along the vertical. Using the shape–size relation and the corresponding back-scatter cross section of raindrops at horizontal and vertical polarization states, models of Z_{dr} and K_{dp} in rain have been developed to study the microphysics of rainfall from these measurements. The differential reflectivity measurement yields a good measure of the volume-weighted drop median diameter D_o. Similarly, K_{dp} is proportional to the product of water content (W) and mass-weighted mean diameter D_m (Jameson 1985). These intrinsic microphysical properties have been utilized extensively in the literature for various applications, including retrieval of DSD parameters and rainfall estimation. Several laboratory experiments as well as measurements of free-falling raindrops have essentially confirmed that the raindrop shapes are in the general region suggested by Beard and Chuang (Chandrasekar et al. 1988; Kubesh and Beard 1993; Bringi et al. 1998; Andsager et al. 1999; Gorgucci et al. 2000; Thurai and Bringi 2005).

approximation to the axis ratio of raindrops approximating the shape of oblate spheroids as

$$\frac{b}{a} = 1.03 - 0.062D, \qquad 1 \le D \le 9 \text{mm}. \qquad (3)$$

DSD retrievals. A long-standing pursuit of polarimetric radar applications has been the retrieval of raindrop size distribution. Early studies focused on
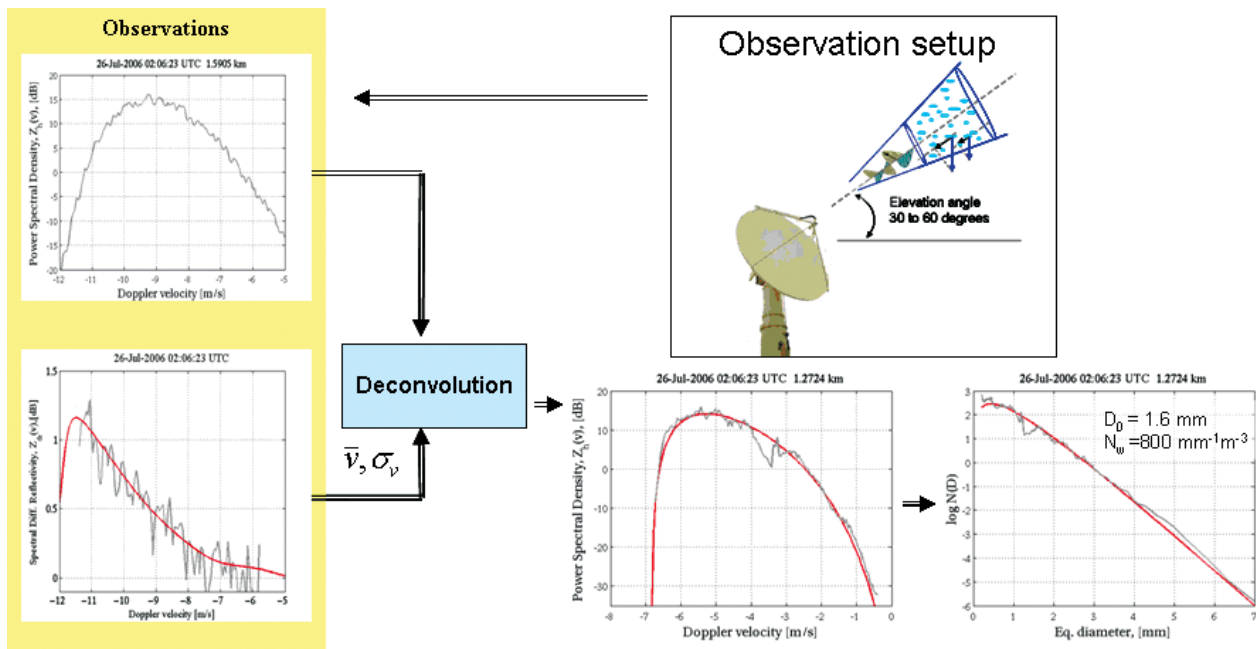

FIG. 4. Block diagram of nonparametric DSD estimation process. The term nonparametric refers to the absence of a specific parametric form of the DSD, such as exponential or gamma. Spectral differential reflectivity is used to estimate radial projection of ambient air velocity and spectral broadening kernel width (Moisseev and Chandrasekar 2007). Then using this information the deconvolution procedure is applied to the observed Doppler power spectrum. The deconvolved spectrum can directly be related to a DSD and yields estimated DSD. In the figure above, the gray solid lines show measurements; the red lines give best fit to the data.

the estimates of drop median diameter D_o or the mass-weighted mean diameter D_m. Fairly simple power-law-based retrievals have been developed in the literature both based on theoretical considerations as well as empirical deductions (Seliga and Bringi 1976; Aydin et al. 1987; Goddard and Cherry 1984). Therefore dual-polarization measurements provide fairly simple retrievals of DSD parameters. Gorgucci et al. (2001, 2002) developed algorithms for retrieving rain rate (R) as well as the parameters of a gamma DSD, namely, D_o, N_w, and μ using the effective shape concept in combination with the measurement pair (Z_h, Z_{dr}). The functional relationship between Z_{dr} and D_o is developed from the underlying microphysical relation between the mean axis ratio of raindrops and their size.

Once D_o is retrieved, then the other parameters of the DSD can be retrieved, such as the intercept of the normalized form of a gamma distribution (Gorgucci et al. 2002). The statistics of the parameter sets D_o, N_w are important in the development of algorithms. Bringi et al. (2003) used the DSD retrieval method to scale the process to world-wide application over different climatic regimes. While the above are parametric retrievals, nonparametric retrievals of DSDs are also possible combining the advantages of a Doppler and polarimetric radar as demonstrated by Moisseev and Chandrasekar (2007). Figure 4 shows the nonparametric DSD retrieval from dual-polarization spectral analysis.

The variability of the DSD across different climatic regimes can be demonstrated by examining the variability of mean $<N_w>$ versus mean $<D_m>$, where angle brackets denote averages. For example, Fig. 5a shows such data retrieved from disdrometer measurements as well as from polarimetric radar data for stratiform rain. A large extent of the data for Fig. 5 came from the globally diverse ground validation observations of the TRMM program. For stratiform rain there appears to be a clear inverse relation between $\log_{10}(<N_w>)$ and $<D_m>$; in fact, it is quite remarkable that a straight-line fit results from the composite disdrometer and radar retrievals, these data encompassing a number of regimes from near equatorial to the U.S. High Plains. From a microphysical perspective, stratiform rain results via the melting of snowflakes and/or tiny graupel or rimed particles. If the bright-band is "strong," then it likely reflects melting of larger, low-density and dry snowflakes into relatively larger raindrops, whereas if the bright band is "weak" then it may reflect the melting of tiny, compact graupel or rimed snow particles (Waldvogel et al. 1995). In essence, the large, low-
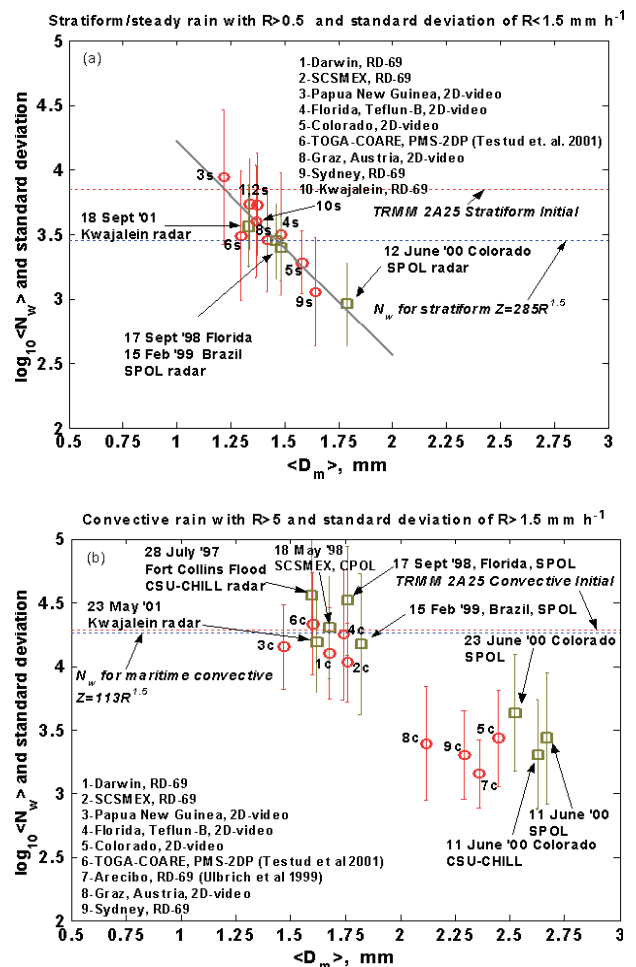

FIG. 5. The average value of $\log_{10}(N_w)$ (with ±1σ standard deviation bars) vs average D_m from disdrometer data and radar retrievals as indicated for (a) stratiform rain and (b) convective rain. Also, the blue dashed horizontal lines at constant $\log_{10}(N_w)$ are the values used for stratiform and convective fixed Z–R relations, while the red dashed ones are derived from TRMM 2A25 initial values. Note that the unit of N_w is mm^{-1} m^{-3}.

density snowflakes lead to DSDs that have smaller $<N_w>$ and larger $<D_m>$ relative to the tiny, compact graupel or rimed snow particles.

Figure 5b shows similar results for convective rain. There appears to be a cluster of data points with $<D_m>$ = 1.5–1.75 mm and $\log_{10}<N_w>$ = 4–4.5, the regime varying from near equatorial (Papua New Guinea) to subtropics (Florida, Brazil) to oceanic [Tropical Ocean and Global Atmosphere Coupled Ocean–Atmosphere Response Experiment (TOGA COARE), Kwajalein, South China Sea Monsoon Experiment (SCSMEX)]. This cluster may be referred to as a "maritime"-like cluster where rain DSDs are characterized by a higher concentration of smaller-sized drops. The Fort Collins flash flood

event is unusual for Colorado as the data fall in the maritime-like cluster. The vertical structure of reflectivity in this event was highly unusual for summertime Colorado storms, resembling instead the vertical profile of Z in oceanic convection (Petersen et al. 1999).

The second "cluster" is characterized by $<D_m> = 2–2.75$ mm and $\log_{10}<N_w> = 3–3.5$, the regime varying from the U.S. High Plains (Colorado) to continental (Graz, Austria) to subtropics (Sydney, Australia) to tropics (Arecibo, Puerto Rico). This cluster may be defined as the "continental" cluster, which reflects rain DSDs characterized by a lower concentration of larger-sized drops as compared with the previously defined maritime-like cluster.

Rosenfeld and Ulbrich (2003) have discussed the microphysical mechanisms contributing to systematic DSD differences using empirical $Z–R$ relations obtained by many observers. Objective rain-type classification has been proposed, among others, by L'Ecuyer et al. (2004) using the 3D structure of Z, which is expected to reduce regime-dependent systematic errors in the rainfall estimates. A different way of classifying vertical profiles of Z is the method using self-organizing maps (SOMs). The SOM is an unsupervised learning neural network that forms a nonlinear mapping of the vertical profile of Z to a 2D map and has been applied to TRMM precipitation radar (PR) datasets on a global scale (Zafar and Chandrasekar 2004). However, the extent to which complex microphysical processes that ultimately lead to the DSD can be identified via only the 3D or 1D vertical structure of Z, though promising, is not as yet fully established. Polarimetric radars will most likely play an important role in answering these questions.

Rainfall estimation and hydrometeor classification. The TRMM era has produced substantial progress in the understanding and application of dual-polarization radar observations of precipitation especially in the tropics. The specific TRMM era deployments are discussed in the "Progress on validation of TRMM precipitation measurement with dual-polarization radars" section, whereas this section discusses the methodologies of dual-polarization radar rainfall estimation algorithms. The various dual-polarized radar measurement parameters that are used in rainfall estimation are reflectivity (say at horizontal polarization Z_h), differential reflectivity (Z_{dr}), and specific differential propagation phase (K_{dp}) (Bringi and Chandrasekar 2001; Ryzhkov et al. 2005). Numerous algorithms have been developed based on a combination of these three measurements. The $Z–R$ algorithms

have been around for a long time, originally developed as statistical regression estimates between Z_h measured by radar and rainfall measured on the ground by gages. The concept of scaling and normalization of DSDs can be used to provide a physical basis for the $Z–R$ relation. The $Z–R$ algorithm is of the form

$$R = cZ^\beta, \qquad (4)$$

where the normalized DSD indicates that c is dependent on N_w, where β is nearly constant. Dual-polarized radar measurements have been used to obtain algorithms for R, which can be generally classified as $R(Z, Z_{dr})$, $R(K_{dp})$, and $R(K_{dp}, Z_{dr})$ algorithms depending upon what variables are used in the estimation. The error structure of these algorithms have been analyzed extensively in the literature and summarized in Chandrasekar and Bringi (1988), Chandrasekar et al. (1990), and Ryzhkov et al. (2005). Under ideal conditions of a perfectly calibrated radar and homogeneous resolution volume the error in these algorithms can be separated into error in the parameterization ε_p, and the error due to measurement inaccuracy in radar observations, ε_m. The $Z–R$ algorithms have large ε_p, whereas all dual-polarization algorithms have small parameterization error. The statement about ε_m is not so straightforward.

Dual-polarization precipitation algorithms yield the best estimates of rain rate for moderate to heavy rainfall. However, in light rain $Z–R$ works fairly well provided the calibration is accurately maintained (Chandrasekar et al. 1990, part 3). It is not useful to further define the performance of these algorithms without considering numerous other factors, such as radar operating frequency, sensitivity to calibration errors, and contamination by ice hydrometeors. In addition to parameterization errors, one of the problems in reflectivity-based estimates is that any bias in the measurement, such as those due to calibration errors or improper attenuation correction will impact rainfall estimates. Any such errors will be recognized as "inconsistencies in the measurement space of the dual-polarization observations," or commonly called lack of "self consistency" of dual-polarization radar observations (Gorgucci et al. 1992; Scarchilli et al. 1996). The ability of dual-polarization radar observations to detect ice particles is also an advantage here, where simple reflectivity-only radar may not be able to do the same. Thus, even the simple reflectivity-based rainfall estimates will also benefit from dual-polarization radar observations. Thus, the renewed awareness of radar calibration brought along by the dual-polarization radar era is not surprising

(Joe and Smith 2001; Notes from Short Course on Weather Radar Calibration, AMS Annual Meeting, San Antonio, Texas, January 2007).

Apart from this, the measurements of K_{dp} and Z_{dr} have their own advantages. Here K_{dp} is obtained from only phase measurements, and they are completely immune to radar calibration problems (as opposed to reflectivity measurements). The advantage of K_{dp} in comparison to Z_h mirrors that of frequency or phase modulation (FM) versus amplitude modulation (AM), because K_{dp} is based on phase measurements. At the same time, similar to the problem of FM when the signal is weak, at low rain rates K_{dp} has large measurement errors. The measurement K_{dp} has numerous advantages as enumerated in Zrnic and Ryzhkov (1996). Similarly, Z_{dr} is a relative power measurement and it can be calibrated to high accuracy compared to reflectivity (Hubbert and Pratte 2007). Thus, K_{dp}- and Z_{dr}-based rainfall estimates are immune to absolute calibration errors. The JPOLE evaluation showed that the polarimetric rainfall algorithms tuned for the JPOLE produced negligible bias as well as lower random error when compared to standard WSR-88D rainfall products.

All the above discussion pertains to pointwise rainfall estimation. The range cumulative differential phase does natural integration of K_{dp}. This feature lends itself to estimation of the area integral of rainfall rate, which can be estimated from direct differential phase measurements instead of having to compute K_{dp}. This technique to compute area integrated of rainfall rate was introduced and evaluated by Raghavan and Chandrasekar (1994), Ryzhkov et al. (2000), and Bringi et al. (2001). These papers clearly demonstrate the advantage of dual-polarization measurements for rainfall estimation. The JPOLE results also show similar advantages.

Numerous experiments have shown the improved estimates of dual-polarization rainfall estimates (Seliga et al. 1981; Aydin et al. 1995; Bringi et al. 2004; Ryzhkov et al. 2005; Schuur et al. 2001); the best advantage has been demonstrated in extreme events such as a flash flood. The polarimetric radar estimates of the Fort Collins flash flood showed clearly that in extreme events the dual-polarization rainfall estimates perform very well (Brandes et al. 1997; Petersen et al. 1999). Figure 6 shows the rainfall accumulation contours of $R(K_{dp}, Z_{dr})$, $R(Z_h, Z_{dr})$, and NEXRAD Z–R to be compared against gage-based contours for the Fort Collins flash flood event. The corresponding rain gauge measurements yielded a peak accumulation of 260 mm; $R(K_{dp}, Z_{dr})$ and $R(Z_h, Z_{dr})$ yielded peak accumulation of 240 and 265 mm, respectively. It can be clearly seen from Fig. 6 that the polarimetric radar algorithms gave the best estimate of rainfall.

A direct application of the polarimetric radar algorithms will be difficult with ice contamination. To account for this, hydrometeor classification and rainfall estimation have been applied together as a combined process to classify precipitation, before quantification. This philosophy has led to the development of blended algorithms (Petersen et al. 1999; Cifelli et al. 2002). As an example, Fig. 7 shows a time series of rainfall over the location of the Urban Drainage and Flood Control District (UDFCD) Automated Local Evaluation in Real Time (ALERT) rain gauge, located near Denver International Airport, on 19 June 2004. The time period shown extends from 1547 local time (170.901 Julian day UTC) to 1633 local time (170.942 Julian day UTC). The green line shows the actual rain gauge trace and the red and black lines represent rain-rate estimates over the gauge using CHILL radar data in combination with the standard NEXRAD Z–R relationship (red line) and blended polarimetric algorithm as discussed above (black line). The latter method makes use of Z_{dr} and K_{dp}, in addition to Z_h, to determine the optimum rainfall estimator at each grid point in the radar domain. The symbols represent the most probable hydrometeor type in the radar volume over the location of the UDFCD rain gauge, based on hydrometeor classification: "R" represents rain and "WG" represents wet graupel. Note that the polarimetric algorithm does a much better job at reproducing the gauge estimate of rainfall, compared to the standard reflectivity-based technique. Because the blended algorithm utilizes differential phase and differential reflectivity information in addition to Z_h, it can detect the likely presence of precipitation ice (e.g., wet graupel) and adjust the rainfall retrieval algorithm to produce more reliable estimates of rainfall.

Hydrometeor classification. Polarimetric radar measurements are sensitive to the types, shapes, and size distributions as well as fall behaviors of hydrometeors in a radar resolution volume. As a result, extensive information about the microphysics of hydrometeors is contained in the polarization diversity radar measurements. The ability to classify hydrometeors has a wide variety of applications, such as initialization and validation of cloud microphysical models, choice of the right algorithm for precipitation estimation, and evaluation of assumptions made in the precipitation retrieval processes. The mapping from polarimetric radar measurement space and

hydrometeor-type space is not one to one. Over the last two decades numerous advances have been made in the area of hydrometeor identification in specific storm types. Liu and Chandrasekar (1998, 2000)

evaluated a variety of techniques, such as the decision tree, statistical decision theory, neural networks, and fuzzy logic and presented arguments for synthesizing all the knowledge base of polarimetric radar measurements, using fuzzy logic to perform robust, hydrometeor classification. They also developed a fuzzy hydrometeor classification system and presented results from in situ validation experiments using data from the T-28 storm penetration aircraft and CSU–CHILL radar data. Vivekanandan et al. (1999) have presented a synthesis of polarimetric radar measurement properties for hydrometeor classification. Straka et al. (2000) summarized microphysical properties of precipitation for hydrometeor classification. Since these early studies, numerous researchers have reported advances in hydrometeor classification using polarimetric radar observations to the point it is becoming a fairly mature area of research. One of the major differences in application of hydrometeor classification for WSR-88D and spaceborne applications is the emphasis on the full vertical structure of hydrometeor classification.

Operational hydrometeor classification systems, such as those proposed for the WSR-88D, work on plan position indicators (PPIs) of dual polarization radar measurements (Ryzhkov et al. 2005; Keranen et al. 2007). The spaceborne radar observations of precipitation have excellent vertical resolution; hence the cross validation with hydrometeor classifications have focused more on ground-based radar operation in range height indicator (RHI) mode. The RHI mode gets instantaneous vertical structure of dual-polarization measurements in contrast to a reconstructed profile over a 5-min volume scan. With such high resolution, Lim et al. (2005) have been able to map the varying transition of the ice/water boundary as shown in Fig. 8. Such high-resolution RHI scans and the corresponding hydrometeor classification are best suited for cross validation with spaceborne measurements. However, the reconstructed volume scans can also be used if the cross validation can work with the reduced resolution of a reconstructed vertical profile from PPI volume scans.
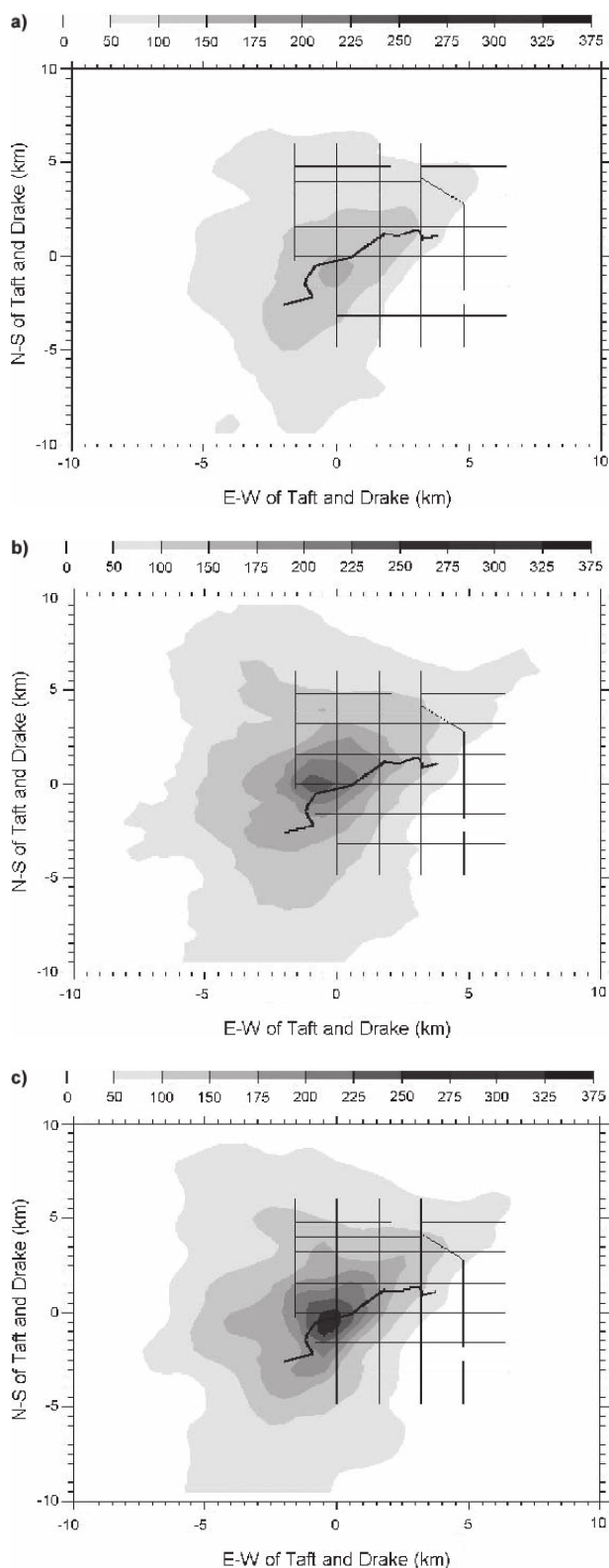
Fig. 6. Storm-total rainfall in mm from 1730 to 2215 MDT. The lines on the picture indicate the street map of the city of Fort Collins. The dark line shows the Spring Creek, which flooded and caused the flash food. (a) $R_{WSR}(Z)$ estimate, (b) $R(K_{dp}, Z_{dr})$ estimate, and (c) $R(Z_h, Z_{dr})$ estimate (Petersen et al. 1999). The peak accumulation recorded by the rain gauge is 260 mm. $R(K_{dp}, Z_{dr})$ and $R(Z_h, Z_{dr})$ yielded a peak accumulation of 240 and 265 mm, respectively.

Currently there are two independently developed models for hydrometeor classification, namely, the CSU model and the NCAR/NSSL model. Though the basic principles of these models are similar, the two models have been developed with different underlying philosophies, namely, the CSU model separates the data quality and hydrometeor classification processes, whereas the NCAR/NSSL model combines them. Recently Lim et al. (2005) further developed the CSU model by striking a compromise between the properties of the original CSU model and NCAR/NSSL model, which essentially balances the metrics of probability of error and false positive classification. This new model also introduced the use of varying melting level information to the hydrometeor classification process. The CSU model puts out fewer classes compared to the NCAR/NSSL model. Based on the arguments presented in Liu and Chandrasekar (2000), such as robustness, and simplicity of implementation and simplicity of adapting a common framework for regional and seasonal variabilities, such as summer, winter, continental, and oceanic, fuzzy-logic-based hydrometeor classification scheme is becoming widely popular to the point that it is being applied to operational systems (Keranen et al. 2007; Petersen et al. 2007).
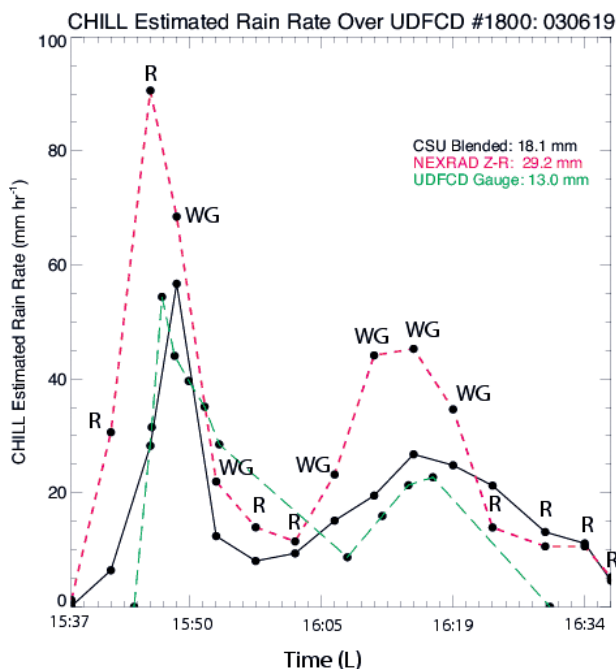
PROGRESS ON VALIDATION OF TRMM PRECIPITATION MEASUREMENT WITH DUAL-POLARIZATION RADARS. The TRMM precipitation radar records energy reflected from precipitation and surface targets. The PR is a 128-element active phased array system operating at 13.8 GHz. The PR electronically scans from right to left, looking in the flight direction across the ground track of the satellite every 0.6 s, with horizontal resolution at the ground of 4.3 km and a swath width of 215 km
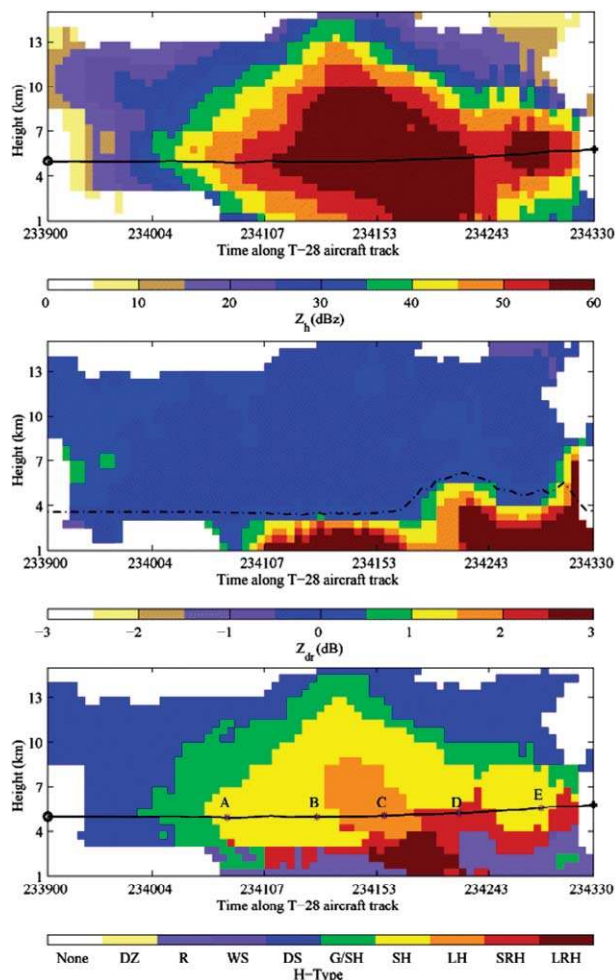

FIG. 7. A time series of rainfall over the location of the **UDFCD ALERT** rain gauge, located near Denver International Airport, on 19 Jun 2004. The symbols represent most probable hydrometeor type in the radar volume over the location of the **UDFCD** rain gauge based on hydrometeor classification. Here **R** represents rain and **WG** represents wet graupel.

FIG. 8. Vertical structure of radar measurements (Z_h, Z_{dr}) and the hydrometeor classification result corresponding to the case of 29 Jun 2000. The vertical section data are generated from a ~5-min PPI volume scan observed by **CSU–CHILL** radar during the **Severe Thunderstorm Electrification and Precipitation Study (STEPS)**. Dotted line in Z_{dr} field is the detected melting level using vertical profiles of Z_h and Z_{dr}. DZ, R, WS, DS, G/SH, SH, LH, SRH, and LRH represent drizzle, rain, wet snow, dry snow, graupel and/or small hail, small hail, large hail, small rain/hail mixture, and large rain/hail mixture, respectively. Adopted from Lim et al. 2005.
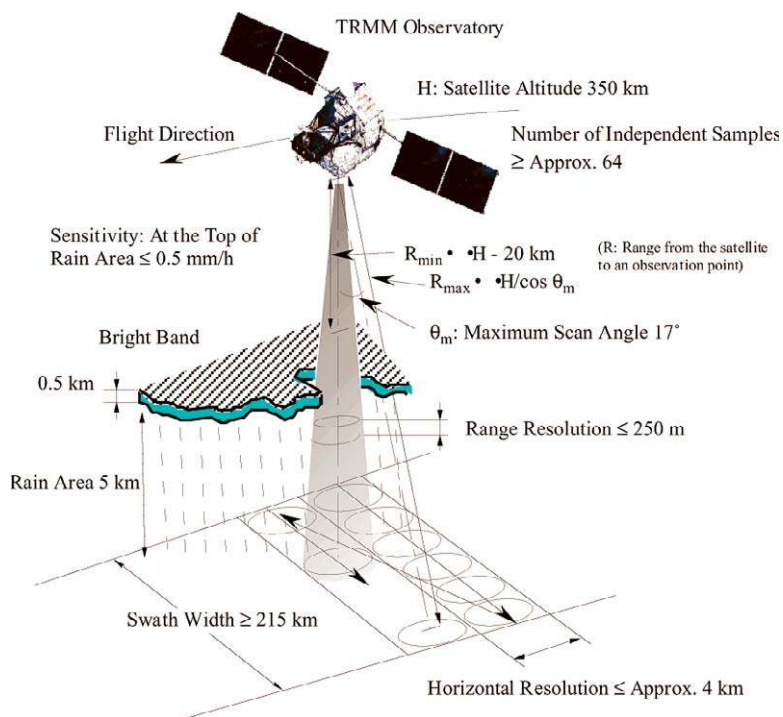
Fig. 9. The observation concept of the PR (adopted from TRMM Precipitation Radar Instruction Manual 2004).

TABLE 1. Precipitation radar parameters (adopted from TRMM Precipitation Radar Instruction Manual 2004).	
Radar type	Active phased array radar
Frequency	13.796 and 13.802 GHz (two-channel frequency agility)
Swath width	About 215 km
Observable range	Over 20 km
Range resolution	250 km
Horizontal resolution	4.3 km (nadir)
Sensitivity	S/N per pulse ≥ 0 dB for 0.5 mm h^{-1} rain at rain top
Independent samples	64
Data rate	93.5 kbps
Weight	465 kg
Power	213 W
Antenna type	128-element slotted wave guide array antenna
Beam width	0.71° × 0.71°
Aperture	2.1 m × 2.1 m
Scan angle	±17°
Gain	About 47.4 dB
Transmitter type	Solid State Power Amplifier (SSPA) and Low Noise Amplifier (LNA) (128 channels)
Peak power	Over 700 W
Pulse width	1.6 μsec × 2 ch
Pulse repetition frequency	2776 Hz
Dynamic range	About 81.5 dB

(Fig. 9). Each PR scan contains 49 rays sampled over an angular sector of 34°. For any given ray, the instrument begins recording samples at a fixed distance from the satellite and records a certain number of samples along the ray. The starting distance and the number of samples are different for each ray. Rays other than the nadir ray also sample below the ground surface. The purpose of this extension below the surface is to clearly detect the location of the surface.

The TRMM satellite has a circular nonsynchronous orbit with an altitude of approximately 350 km. This orbit allows the TRMM satellite to pass over each part of the surface of the Earth at a different local time daily. The precipitation radar parameters are listed in Table 1. Iguchi et al. (2000) describe the details of the algorithms used by TRMM PR for attenuation correction and rainfall estimation. Similarly Kummerow et al. (2000) describe the radiometer algorithm for rainfall estimation. The basic principle of the TRMM PR algorithm is described in Fig. 10. The fundamental assumptions of the TRMM PR retrieval is the attenuation and rainfall rate are modeled as power laws with reflectivity governed by the propagation integral equation using the surface reference as boundary condition. The path-integrated attenuation estimate is subsequently used to tune the coefficients of the power-law relations used between reflectivity and attenuation. The attenuation-corrected reflectivity is used for rainfall estimate. The TRMM PR algorithm (commonly referred to as 2A25) also

adjusts for nonuniform beam filling (NUBF). When the rainfall rate is low the surface reference is not reliable to compute the total attenuation and a simple iterative model is used for attenuation correction and rainfall estimation.

The TRMM program operates many validation sites around the globe. In addition, extensive field campaigns were also conducted. Among the validation sites, the site in Darwin, Australia, has operated a C-band dual-polarization Doppler radar (C-POL) for an extended period. In addition, the C-POL radar was deployed during the SCSMEX. Substantial contributions to rain microphysics and rainfall algorithm development were contributed by research and observations from this site. The impact of raindrop oscillations and K_{dp}-based rainfall algorithm for tropics were demonstrated fairly early from this site (Keenan et al. 1998). These concepts were further developed into fundamental contributions to rainfall microphysics. The C-POL data were also used to validate the rain-profiling algorithm developed for ground polarimetric radars. Among the other sites, the Texas and Florida Underflights Experiment (TEFLUN-B) and the TRMM Large-Scale Biosphere–Atmosphere Experiment (TRMM LBA) both had full deployment of the National Center for Atmospheric Research S-POL radar, which is an S-band dual-polarization Doppler radar (Carey et al. 2001; Cifelli et al. 2004; Chandrasekar et al. 2003). Both deployments resulted in development of methodologies for interpretation of PR observations, evaluation of DSD assumptions, precipitation regime classification, validation of PR attenuation correction algorithms, and area rainfall estimates. Nakagawa et al. (2004) presented similar applications from the ground site in Okinawa.

In addition, a series of coordinated comparisons have been made between TRMM PR observations and ground polarimetric radar. Chandrasekar et al. (2003) conducted careful pointwise comparisons between TRMM PR and ground radar (GR) to show the potential of ground polarimetric radars to assess the attenuation correction process based on common data framework between ground radars and TRMM
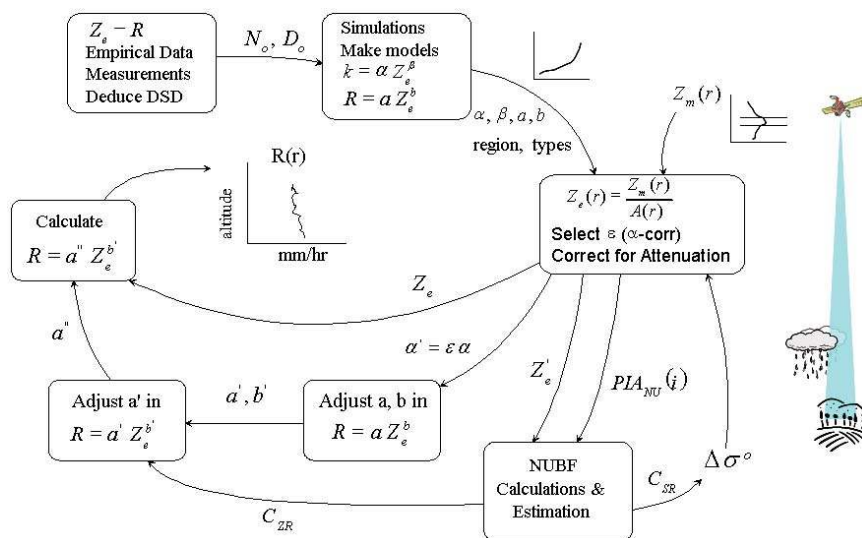

FIG. 10. The basic principle of the TRMM PR algorithm. The key features of the algorithm are 1) surface reference technique, 2) attenuation correction, and 3) NUBF correction and subsequent rainfall estimation based on Z–R algorithm (Rose and Chandrasekar 2007).

PR (Bolen and Chandrasekar 2003). Figure 11 shows the schematic of comparing spaceborne and ground-based radar observations. Figures 12a and 12b show a vertical profile comparison of the various parameters measured by the ground polarimetric radar, such as reflectivity, differential reflectivity, LDR, and copolar correlation, namely, compared against the TRMM radar observations. Similar comparisons with C-band polarimetric radars are shown in Fig. 12c. These comparisons were used to evaluate the accuracy of attenuation correction done by the operational TRMM PR algorithm. Direct intercomparison between TRMM PR and ground-based radar is a challenging task.
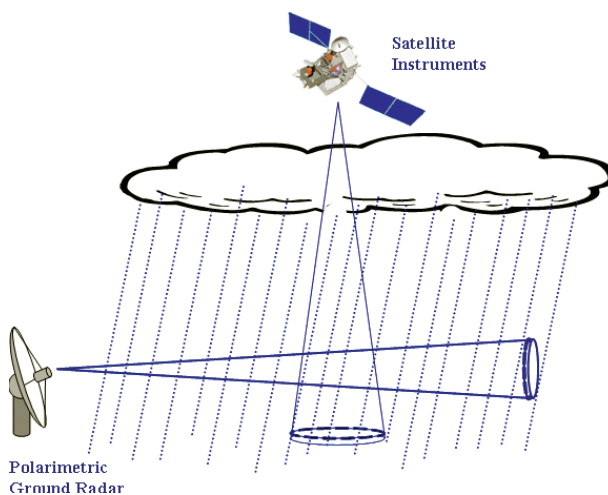

FIG. 11. A schematic comparing spaceborne and ground-based radar observations.

Difference in viewing aspects between Earth and space observations, propagation paths, frequencies, resolution volume size, and time synchronization mismatch between space and ground-based observations can contribute to discrepancies in point-by-point intercomparison (Bolen and Chandrasekar 2003). TRMM PR has been remarkably stable with respect to calibration of the system as evidenced by the active radar calibrator (Akihiro et al. 2004). The Active Radar Calibrator (ARC)-based calibration system established the TRMM PR calibration to an accuracy of within 1 dB. With the TRMM PR being very stable and with advanced cross-validation procedures, which account for frequency difference, view angle, distortion, etc., the cross validation can be really used for algorithm performance evaluation.

The normalized gamma DSD model was used by Chandrasekar et al. (2003) to conduct microphysical comparisons on a pixel basis from TRMM PR and ground polarimetric radar. The D_o retrieval algorithm was presented in their paper. This concept was extended to a global scale where global maps of DSD estimates were constructed in Chandrasekar et al. (2005). This global map is a further scale-up of the DSD reported from different climatic region by Bringi et al. (2003). Wilheit et al. (2007) have shown
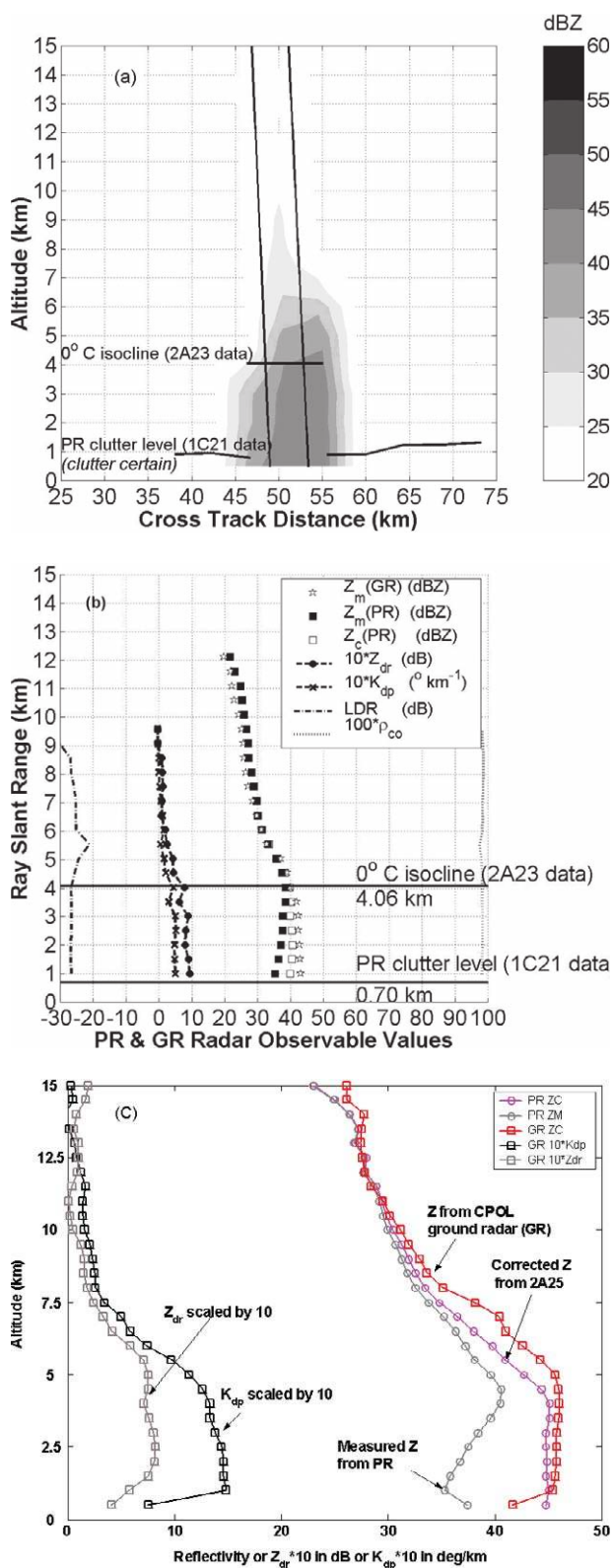

Fig. 12. Example of ground-based observations and RSD estimates from data using TRMM LBA. (a) Vertical profile of GR reflectivity with location of PR beam indicated by solid vertical lines drawn to scale. (b) GR polarimetric observations along PR ray corresponding to the ray as indicated in (a). From left to right, the dashed line is LDR, solid line with x's is K_{dp} (scaled by a factor of 10), solid line with circles is Z_{dr} (scaled by 10), black squares are PR measured (attenuated) reflectivity, white squares are PR attenuation corrected reflectivity, stars are GR measured reflectivity, and the dotted line is the cross-correlation coefficient between GR return signal horizontal and vertical polarization states, ρ_{co} (scaled by 100). In this plot, PR attenuation is observed to be about 7 dB with reference to GR measurements. In all panels, solid horizontal lines indicate the 0°C isocline altitude and the PR clutter level (certain), as derived from the TRMM data products, respectively. These types of profiles were used to evaluate the accuracy of attenuation correction by the TRMM operational algorithm, while the accompanying dual-polarization measurements provide auxiliary information about the prevailing microphysics for interpretation of the cross validation. (c) The (horizontally averaged) vertical profile of measured and corrected reflectivity from PR along with Z_h, Z_{dr}, and K_{dp} from the C-Pol GR. These data are for the Darwin ocean event of 3 Feb 2000. The Z match is quite good; it can be noted that average Z_{dr} in the lower rain layer is around 0.8 dB, with K_{dp} reaching 1.5° km^{-1}, indicating, on average, a maritime DSD with larger concentration of relatively smaller size. The scope of the comparison is similar to Fig. 12b.

the utility of such global maps for development of passive microwave remote sensing algorithms from satellite observations.

In summary, the limited use of dual-polarization radars during the TRMM era have yielded substantial benefits in numerous areas, including a) validation of TRMM PR attenuation correction algorithms, b) precipitation regime classification, and c) fundamental advances in the understanding of rain microphysics in terms of differences between continental and oceanic events as well as convective and stratiform storms.

POTENTIAL APPLICATION OF DUAL-POLARIZATION RADAR FOR GPM. The application of dual-polarization radars to GPM era precipitation measurements is discussed in the following. Specifically, the combined DPR and GMI precipitation measurements made from the GPM core satellite form the nexus of a spaceborne precipitation "validation" tool to be used for calibrating the entire GPM constellation. Hence to a large extent, validation of the GPM core satellite precipitation retrievals ensures overall measurement fidelity and accuracy of the entire GPM constellation. When the validation process is conducted at the ground in widely varying precipitation environment types, the methodology can leverage several of the intrinsic capabilities associated with dual-polarization radar, including 1) self-consistent calibration; 2) improved detection of hydrometeor phase, shape, and type; 3) retrieval of particle size distribution information; and 4) via capabilities 1–3, improved accuracy in retrieved precipitation rate (on both instantaneous and integrated time scales). Collectively, these capabilities support GPM ground validation approaches ranging from large-scale national network statistical validation of GPM precipitation estimates, to detailed physical validation of GPM satellite algorithms at precipitation and microphysical process scales.

At national network scales, several countries/ regions around the world have recognized the increased capability of dual-polarimetric radar (i.e., the four capabilities described above) for QPE and are already pursuing dual-polarization upgrades. Specific examples include the WSR-88D program in the United States, the European Weather Radar Network, and the ground radar network of the Meteorological Service of Canada. For these operationally driven radar networks data quality and calibration monitoring leading to improved QPE are two of the most important attributes associated with polarimetric upgrades. Relative to GPM, the improved quality of

the precipitation measurement provided by the new dual-polarimetric radar networks should result in more widespread, accurate precipitation measurements with lower standard error over many locations of the globe, thereby significantly increasing confidence in the ground component (i.e., ground "truth") of the satellite–ground QPE comparison.

From a physical validation perspective, the combination of DSD parameter retrievals and hydrometeor classification facilitated by dual-polarization radars provides an important means to cross-validate microphysical properties parameterized in evolving GPM DPR and GMI retrieval algorithms. As stated above, the suite of polarimetric variables provides the means to internally calibrate/correct/ assure a given reflectivity estimate, and this can be done for multiple dual-polarimetric radars in a given network, such that a "uniform" calibration standard for the network is attained. In turn, the radar network reflectivity estimates form a collectively calibrated dataset that can be compared directly to DPR reflectivities (assuming consistent comparison geometries). When continuously collected and archived, these comparison points, especially those comparison points deemed to be most reliable, compose the core of a dataset that can be statistically analyzed to provide a robust validation of the DPR calibration and attenuation correction. In the process of this direct statistical validation of DPR reflectivities it should be possible to discern specific regions and/or meteorological situations where there is a significant mismatch between the ground and spaceborne measurements. In this instance, specific research-grade multifrequency polarimetric radars can be deployed for use in an intensive observation mode (i.e., free to scan any 3D volume of space at variable frequency as needed) to examine the reflectivity, precipitation rates, and characteristics in the "discrepancy" regimes or regions. This particular part of the physical validation process need not rely heavily on DPR overpasses to accomplish the DSD validation relative to meteorological regime, radar reflectivity, and precipitation rate.

From a quantitative perspective the retrieval of parameters related to DSD properties (e.g., D_o, N_w, etc.) and precipitation rate using advanced dual-polarimetric radar techniques is of great interest to programs such as GPM. However, it is also true that the accurate retrieval of these properties using dual-polarization radar can be problematic and subject to error if the measurements and/or analyses are not done carefully. Importantly, even if one questions the validity of quantitative DSD retrievals for

a given radar, there remain *qualitative* aspects of the dual-polarimetric measurements that lend themselves readily to precipitation retrieval algorithm validation. For example, at the most basic qualitative level the fundamental ability of dual-polarization radar to distinguish between liquid, ice, and mixed water phases in the vertical structure of precipitation is likely to play a crucial role in the development of both dual-frequency radar algorithms as well as combined radar–radiometer algorithms. The delineation between the water phases is currently an outstanding problem in the retrieval of precipitation rates from passive microwave sensors. To this end, cloud-resolving models capable of generating realistic synthetic hydrometeor profiles, including the mixed phase, are important to the process of algorithm development and testing. As part of this process dual-polarization radar-diagnosed profiles of hydrometeors and hydrometeor phases can be linked to radar-derived precipitation rates and then used to verify the general characteristics of simulated cloud model microphysics used in the algorithm development process.

In summary, the ability of the dual-polarization radar to supply both basic qualitative information related to hydrometeor phase/type information (in three dimensions) coupled with the potential for more advanced quantitative retrieval of DSD properties is of great interest to GPM. It is also important to note that because the aforementioned data are typically collected by polarimetric radars possessing scanning agility, variable area coverage, and temporal continuity of operation (especially true of research radars), the data represent more than just "snapshot" retrievals of the precipitation. Samples of the precipitation characteristics and rates can be retrieved over the entire life cycle of given precipitation events and over large areas, making dual-polarimetric radar a valuable analytic instrument for future GPM applications.

REFERENCES

Akihiro, M., T. Nobuhiro, K. Hiroshi, and T. Toyoyuki, 2004: Calibration of the TRMM Precipitation Radar using the active radar calibrator (ARC). *J. Remote Sens. Soc. Japan,* **24,** 367–377.

Andsager, K., K. V. Beard, and N. F. Laird, 1999: Laboratory measurements of axis ratios for large raindrops. *J. Atmos. Sci.,* **56,** 2673–2683.

Aydin, K., H. Direskeneli, and T. A. Seliga, 1987: Dual-polarization radar estimation of rainfall parameters compared with ground-based disdrometer measurements: October 29, 1982, Central Illinois experiment. *IEEE Trans. Geosci. Remote Sens.,* **GE-25,** 834–844.

——, V. N. Bringi, and L. Liu, 1995: Rain-rate estimation in the presence of hail using S-band specific differential phase and other radar parameters. *J. Appl. Meteor.,* **34,** 404–410.

Beard, K. V., and C. Chuang, 1987: A new model for the equilibrium shape of raindrops. *J. Atmos. Sci.,* **44,** 1509–1524.

Bolen, S. M., and V. Chandrasekar, 2003: Methodology for aligning and comparing spaceborne radar and ground-based radar observations. *J. Atmos. Oceanic Technol.,* **20,** 647–659.

Brandes, E. A., J. Vivekanandan, and J. W. Wilson, 1997: Radar rainfall estimates of the Buffalo Creek flash flood using WSR-88D and polarimetric radar data. Preprints, *28th Conf. on Radar Meteorology,* Austin, TX, Amer. Meteor. Soc., 123–124.

Bringi, V. N., and V. Chandrasekar, 2001: *Polarimetric Doppler Weather Radar: Principles and Applications.* Cambridge University Press, 636 pp.

——, ——, and R. Xiao, 1998: Raindrop axis ratios and size distributions in Florida rainshafts: An assessment of multiparameter radar algorithms. *IEEE Trans. Geosci. Remote Sens.,* **36,** 703–715.

——, G.-J. Huang, V. Chandrasekar, and T. D. Keenan, 2001: An areal rainfall estimator using differential propagation phase: Evaluation using a C-band radar and a dense gauge network in the tropics. *J. Atmos. Oceanic Technol.,* **18,** 1810–1818.

——, V. Chandrasekar, J. Hubbert, E. Gorgucci, W. L. Randeu, and M. Schoenhuber, 2003: Raindrop size distribution in different climatic regimes from disdrometer and dual-polarized radar analysis. *J. Atmos. Sci.,* **60,** 354–365.

——, T. Tang, and V. Chandrasekar, 2004: Evaluation of a new polarimetrically based *Z–R* relation. *J. Atmos. Oceanic Technol.,* **21,** 612–623.

Carey, L. D., R. Cifelli, W. A. Petersen, S. A. Rutledge, and M. A. F. Silva Dias, 2001: Characteristics of Amazonian rain measured during TRMM-LBA. Preprints, *30th Int. Conf. on Radar Meteorology,* Munich, Germany, Amer. Meteor. Soc., 682–684.

Chandrasekar, V., and V. N. Bringi, 1988: Error structure of multiparameter radar and surface measurements of rainfall. Part I: Differential reflectivity. *J. Atmos. Oceanic Technol.,* **5,** 783–795.

——, W. A. Cooper, and V. N. Bringi, 1988: Axis ratios and oscillations of raindrops. *J. Atmos. Sci.,* **45,** 1323–1333.

——, V. N. Bringi, N. Balakrishnan, and D. S. Zrnic, 1990: Error structure of multiparameter radar and surface measurements of rainfall. Part III: Specific differential phase. *J. Atmos. Oceanic Technol.,* **7,** 621–629.

——, S. M. Bolen, and E. Gorgucci, 2003: Microphysical cross validation of spaceborne radar and ground polarimetric radar. *IEEE Trans. Geosci. Remote Sens.,* **41,** 2153–2165.

——, W. Li, and B. Zafar, 2005: Estimation of raindrop size distribution from spaceborne radar observations. *IEEE Trans. Geosci. Remote Sens.,* **43,** 1078–1086.

Chang, A. T. C., L. S. Chiu, C. Kummerow, J. Meng, and T. T. Wilheit, 1999: First results of the TRMM microwave imager (TMI) monthly oceanic rain rate: Comparison with SSM/I. *Geophys. Res. Lett.,* **26,** 2379–2382.

Cifelli, R., W. A. Petersen, L. D. Carey, and S. A. Rutledge, 2002: Radar Observations of the Kinematic, Microphysical, and Precipitation Characteristics of Two MCSs in TRMM-LBA. *J. Geophys. Res,* **107,** doi:10.1029/2000JD0000264.

——, L. C. Carey, W. A. Petersen, and S. A. Rutledge, 2004: An ensemble study of wet season convection in Southwest Amazon: Kinematics and implications for diabatic heating. *J. Climate,* **17,** 4692–4707.

Doviak, R. J., V. Bringi, A. Ryzhkov, A. Zahrai, and D. Zrnic, 2000: Considerations for polarimetric upgrades to operational WSR-88D radars. *J. Atmos. Oceanic Technol.,* **17,** 257–278.

Goddard, J. W. F., and S. M. Cherry, 1984: The ability of dual-polarization radar (copolar linear) to predict rainfall rate and microwave attenuation. *Radio Sci.,* **19,** 201–208.

Gorgucci, E., G. Scarchilli, and V. Chandrasekar, 1992: Calibration of radars using polarimetric techniques. *IEEE Trans. Geosci. Remote Sens.,* **30,** 853–858.

——, ——, and ——, 2000: Measurement of mean raindrop shape from polarimetric radar observations. *J. Atmos. Sci.,* **57,** 3406–3413.

——, ——, ——, and V. N. Bringi, 2001: Rainfall estimation from polarimetric radar measurements: Composite algorithms immune to variability in raindrop shape-size relation. *J. Atmos. Oceanic Technol.,* **18,** 1773–1786.

——, V. Chandrasekar, V. N. Bringi, and G. Scarchilli, 2002: Estimation of raindrop size distribution parameters from polarimetric radar measurements. *J. Atmos. Sci.,* **59,** 2373–2384.

Hubbert, J., and F. Pratte, 2007: Differential reflectivity calibration for NEXRAD. *Proc. IGARSS 2006,* Denver, CO, IGARSS, 519–522.

Iguchi, T., T. Kozu, R. Meneghini, and K. Okamoto, 2000: A new hybrid surface reference method for the TRMM Precipitation Radar. *Proc. IGARSS 2000,* Honolulu, HI, IGARSS, 1346–1348.

Jameson, A. R., 1985: Microphysical interpretation of multi-parameter radar measurements in rain. Part III: Interpretation and measurement of propagation differential phase shift between orthogonal linear polarizations. *J. Atmos. Sci.,* **42,** 607–614.

Joe, P., and P. L. Smith, 2001: Summary of the radar calibration workshop. Preprints, *30th Radar Meteorology Conf.,* Munich, Germany, Amer. Meteor. Soc., 3.1. [Available online at http://ams.confex.com/ams/pdfpapers/21882.pdf.]

Keenan, T., K. Glasson, F. Cummings, T. S. Bird, J. Keeler, and J. Lutz, 1998: The BMRC/NCAR C-Band Polarimetric (C-POL) radar system. *J. Atmos. Oceanic Technol.,* **15,** 871–886.

Keranen, R., E. Saltikoff, V. Chandrasekar, S. Lim, J. Holmes, and J. Selzler, 2007: Real-time hydrometeor classification for the operational forecasting environment. Preprints, *33rd Radar Meteorology Conf.,* Cairns, Australia, Amer. Meteor. Soc., P11B.11. [Available online at http://ams.confex.com/ams/pdfpapers/123476.pdf.]

Kubesh, R. J., and K. V. Beard, 1993: Laboratory measurements of spontaneous oscillations for moderate-size raindrops. *J. Atmos. Sci.,* **50,** 1089–1098.

Kummerow, C., and Coauthors, 2000: The status of the tropical rainfall measuring mission (TRMM) after two years in orbit. *J. Appl. Meteor.,* **39,** 1965–1982.

L'Ecuyer, T. S., C. Kummerow, and W. Berg, 2004: Toward a global map of raindrop size distributions. Part I: Rain-type classification and its implications for validating global rainfall products. *J. Hydrometeor.,* **5,** 831–849.

Lim, S., V. Chandrasekar, and V. N. Bringi, 2005: Hydrometeor classification system using dual-polarization radar measurements: Model improvements and in situ verification. *IEEE Trans. Geosci. Remote Sens.,* **43,** 792–801.

Liu, H., and V. Chandrasekar, 1998: An adaptive neural network scheme for precipitation estimation from radar observations. *Proc. IGARSS 1998,* Seattle, WA, IGARSS, 1895–1897.

——, and ——, 2000: Classification of hydrometeors based on polarimetric radar measurements: Development of fuzzy logic and neuro-fuzzy systems, and in situ verification. *J. Atmos. Oceanic Technol.,* **17,** 140–164.

McCormick, G. C., and A. Hendry, 1975: Principles for the radar determination of the polarization properties of precipitation. *Radio Sci.,* **10,** 421–434.

Moisseev, D. N., and V. Chandrasekar, 2007: Nonparametric estimation of raindrop size distributions from dual-polarization radar spectral observations. *J. Atmos. Ocean. Technol.,* **24,** 847–855.

Nakagawa, K., H. Hanado, S. Sato, and T. Iguchi, 2003: Development of the CRL Okinawa Bistatic Polarimetric Radar. *J. Commun. Res. Lab.,* **49,** 225–231.

——, ——, N. Takahashi, S. Satoh, T. Iguchi, and K. Fukutani, 2004: Polarimetric rainfall observations with COBRA in the rainy season. *Proc. Sixth Int. Sympo. on Hydrological Applications of Weather Radar,* Melbourne, Australia, Australian Bureau of Meteorology.

National Research Council, 2006: *Assessment of the Benefits of Extending the Tropical Rainfall Measuring Mission.* National Academies Press, 103 pp.

——, 2007: *NOAA's Role in Space-Based Global Precipitation Estimation and Application.* National Academies Press, 142 pp.

Parent, J., P. Tabary, and M. Guimera, 2005: The Panthere project and the evolution of the French operational radar network and products: Rain-estimation, Doppler winds and dual-polarisation. Preprints, *32nd Conf. on Radar Meteorology,* Albuquerque, NM, Amer. Meteor. Soc., 14R.6. [Available online at http://ams.confex.com/ams/pdfpapers/96217.pdf.]

Petersen, W. A., and Coauthors, 1999: Mesoscale and radar observations of the Fort Collins flash flood of 28 July 1997. *Bull. Amer. Meteor. Soc.,* **80,** 191–216.

——, K. R. Knupp, D. J. Cecil, and J. R. Mecikalsi, 2007: The University of Alabama Huntsville THOR Center instrumentation: Research and operational collaboration. Preprints, *33rd Int. Conf. on Radar Meteorology,* Cairns, Australia, Amer. Meteor. Soc.,5.1. [Available online at http://ams.confex.com/ams/pdfpapers/123410.pdf.]

Pruppacher, H. R., and K. V. Beard, 1970: A wind tunnel investigation of the internal circulation and shape of water drops falling at terminal velocity in air. *Quart. J. Roy. Meteor. Soc.,* **96,** 247–256.

Raghavan, R., and V. Chandrasekar, 1994: Multiparameter radar study of rainfall: Potential application to area–time integral studies. *J. Appl. Meteor.,* **33,** 1636–1645.

Rose, C. R., and V. Chandrasekar, 2007: Systems Engineering Analysis of a TRMM PR-Like Rainfall Retrieval Algorithm. *IEEE Trans. Geosci. Remote Sens.,* **45** (2), 426–434.

Rosenfeld, D., and C. W. Ulbrich, 2003: Cloud microphysical properties, processes, and rainfall estimation opportunities. *Radar and Atmospheric Science: A Collection of Essays in Honor of David Atlas,* R. M. Wakimoto and R. Srivastava, Eds., Amer. Meteor. Soc., 237–258.

Ryzhkov, A., D. Zrnic, and R. Fulton, 2000: Areal rainfall estimates using differential phase. *J. Appl. Meteor.,* **39,** 263–268.

——, T. J. Schuur, D. W. Burgess, P. L. Heinselman, S. E. Giangrande, and D. S. Zrnic, 2005: The Joint Polarization Experiment: Polarimetric rainfall measurements and hydrometeor classification. *Bull. Amer. Meteor. Soc.,* **86,** 809–824.

Sachidananda, M., and D. S. Zrnic, 1987: Rain rate estimates from differential polarization measurements. *J. Atmos. Oceanic Technol.,* **4,** 588–598.

Scarchilli, G., E. Gorgucci, V. Chandrasekar, and A. Dobaie, 1996: Self-consistency of polarization diversity measurement of rainfall. *IEEE Trans. Geosci. Remote Sens.,* **34,** 22–26.

Schroth, A., M. Chandra, and P. Meischner, 1988: C-band coherent polarimetric radar for propagation and cloud physics research. *J. Atmos. Oceanic Technol.,* **5,** 803–822.

Schuur, T. J., A. V. Ryzhkov, D. S. Zrnic, and M. Schoenhuber, 2001: Drop size distributions measured by a 2D video disdrometer: Comparison with dual-polarization data. *J. Appl. Meteor.,* **40,** 1019–1034.

Seliga, T. A., and V. N. Bringi, 1976: Potential use of the radar reflectivity at orthogonal polarizations for measuring precipitation. *J. Appl. Meteor.,* **15,** 69–76.

——, and ——, 1978: Differential reflectivity and differential phase shift: Applications in radar meteorology. *Radio Sci.,* **13,** 271–275.

——, ——, and H. H. Al-Khatib, 1981: A preliminary study of comparative measurement of rainfall rate using the differential reflectivity radar technique and a raingauge network. *J. Appl. Meteor.,* **20,** 1362–1368.

Shimizu, S., R. Oki, M. Kachi, M. Kojima, T. Iguchi, and K. Nakamura, 2006: Development and validation of spaceborne dual-frequency precipitation radar for GPM. *Proc. IGARSS 2006,* Denver, CO, IGARSS, 29–31.

Straka, J. M., D. S. Zrnic, and A. V. Ryzhkov, 2000: Bulk hydrometeor classification and quantification using polarimetric radar data: Synthesis of relations. *J. Appl. Meteor.,* **39,** 1341–1372.

Thurai, M., and V. N. Bringi, 2005: Drop axis ratios from a 2D video disdrometer. *J. Atmos. Oceanic Technol.,* **22,** 966–978.

TRMM Precipitation Radar Instruction Manual, cited 2004: Tropical Rainfall Measuring Mission (TRMM) precipitation radar algorithm instruction manual, version 2.0. [Available online at www.eorc.nasda.go.jp/TRMM/document/pr_manual/pr_manual2.pdf.]

Vivekanandan, J., S. M. Ellis, R. Oye, D. S. Zrnic, A. V. Ryzhkov, and J. Straka, 1999: Cloud microphysics retrieval using S-band dual-polarization radar measurements. *Bull. Amer. Meteor. Soc.,* **80,** 381–388.

Waldvogel, A., W. Henrich, and W. Schmid, 1995: Raindrop size distributions and radar reflectivity profiles. Preprints, *Conf. on Radar Meteorology,* Vail, CO, Amer. Meteor. Soc., 26–28.

Wang, Y., and V. Chandrasekar, 2006: Polarization isolation requirements for linear dual-polarization weather radar in simultaneous transmission mode of operation. *IEEE Trans. Geosci. Remote Sens.,* **44,** 2019–2028.

Wilheit, T., V. Chandrasekar, and W. Li., 2007: Impact of uncertainty in the drop size disatribution on oceanic retrievals from passive microwave observations. *IEEE Trans. Geosci. Remote Sens.,* **45,** 3160–3164.

Zafar, B. J., and V. Chandrasekar, 2004: SOM of space borne precipitation radar rain profiles on global scale. *Proc. IGARSS 2004,* Anchorage, IGARSS, 925–928.

Zrnic, D. S., and A. Ryzhkov, 1996: Advantages of rain measurements using specific differential phase. *J. Atmos. Oceanic Technol.,* **13,** 454–464.